ACS APPLIED MATERIALS & INTERFACES

Research Article

www.acsami.org

Molecular Dynamics Investigation of the Adhesion Mechanism Acting between Dopamine and the Surface of Dopamine-Processed Aramid Fibers

Dongliang Chai,[†] Zhimin Xie,*[,†] Youshan Wang,*[,‡] Li Liu,[§] and Young-Jin Yum[∥]

[†]National Key Laboratory of Science and Technology on Advanced Composites in Special Environment, Center for Composite Materials, Harbin Institute of Technology, Harbin 150001, People's Republic of China

[‡]Center for Organic Functional Materials, Harbin Institute of Technology at Weihai, Weihai 264209, People's Republic of China

[§]Department of Chemical Engineering and Technology, Harbin Institute of Technology, Harbin 150001, People's Republic of China

[∥]School of Mechanical Engineering, University of Ulsan, Ulsan 680749, Republic of Korea

ABSTRACT: Dopamine, as a universal material for surface treatment, can effectively improve the surface performance of aramid fibers. However, directly processing the surface of aramid fibers using dopamine currently incurs a high cost. To seek dopamine substitutes, one must first explore the adhesion mechanism responsible for binding the dopamine to the surface of the fiber. In this study, we construct an all-atomic molecular dynamics model of an aramid fiber before and after surface modification using dopamine. A force field based on condensed-phase optimized molecular potentials for atomistic simulation studies (COMPASS) is used. Using it, we analyze the surface adhesion mechanism of polydopamines aggregated by 21 kinds of molecular structures typically found on the surface of aramid fibers. The results show that a clear and smooth interface is formed between the polydopamine nanofilm layer and the surface of the aramid fiber. The high atomic density of the polydopamine in the small interface region is found to be conducive to noncovalent bonds of polydopamines with the surface of the aramid fiber. In addition, we investigate the works of adhesion of the 21 molecular structures typically found on the surface of aramid fibers. The results suggest that the work of adhesion of 5,6-indolequinone is the highest, followed by annular eumelanin molecules with annular planar structure. Straight-chain shaped dimers proved to be the molecules with the highest adhesion ability of the dihydroxyindole chain oligomers. Therefore, there is reason to suppose that more molecular structures (as above) can be formed by processing the surface of aramid fibers using dopamine by controlling the processing conditions. These molecular structures help improve the adhesion ability of the dopamine on the surface of the aramid fiber. Additionally, if these polydopamine molecules with high adhesion ability can be synthesized on a large scale, then new surface-processing materials are possible.

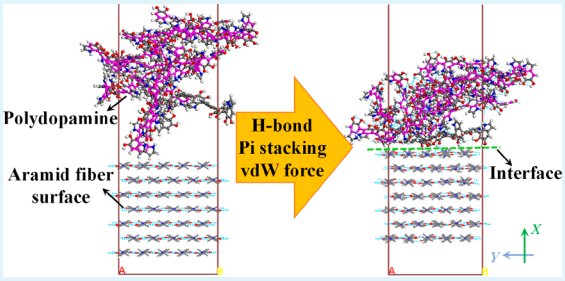

KEYWORDS: *polydopamine, poly(p-phenylene terephthalamide), molecular dynamics, work of adhesion, surface energy*

1. INTRODUCTION

Aramid fibers, an important class of synthetic fibers, are mainly applied in high-performance fabrics and advanced composite materials due to their excellent physical and mechanical properties. However, aramids are greatly restricted by their poor adhesion to substrates when used in composites, which is mainly attributed to their smooth surfaces and high chemical inertness. Therefore, the surface performance of aramid fibers needs to be improved, mainly by increasing the roughness of the surface and modifying active groups on the surface of the aramid fibers. The methods used include etching,[1] surface grafting and polymerization modification,[2] plasma treatment,[3] γ-ray treatment,[4] and ultrasonic treatment.[5] However, these methods of surface treatment also have certain disadvantages. For example, etching tends to damage the aramid fibers and thus reduces the strength of the fibers.[6] Chemical processing requires large amounts of water and chemical agents and thus may result in environmental pollution.[7] High-energy particle treatments have high requirements on equipment and technology. Therefore, seeking simple and efficient surface processing methods for the application of aramid fibers in high-performance composites is of great significance.

Dopamine (DPA) is thought of as a universal material for surface treatment. It is easily oxidized in aqueous solution and the oxidized molecules then adhere to a material's surface in oligomer form where they further polymerize into polydopamine nanofilm layer. Such a film can adhere to the surface of almost all materials,[8] with no exception of superhydrophobic materials with low surface energy.[9] Due to its properties, dopamine has been applied to modify the surface of various

Received: July 21, 2014
Accepted: October 2, 2014
Published: October 2, 2014

ACS Publications © 2014 American Chemical Society

materials, e.g., carbon nanotubes,[10] carbon fiber,[11] and aramid fibers.[9] Recently, we have obtained the surface-modified aramid fibers by immersing the fibers in 2 g/L dopamine solution at 25 °C for 24 h. Figure 1 shows scanning electron microscopy

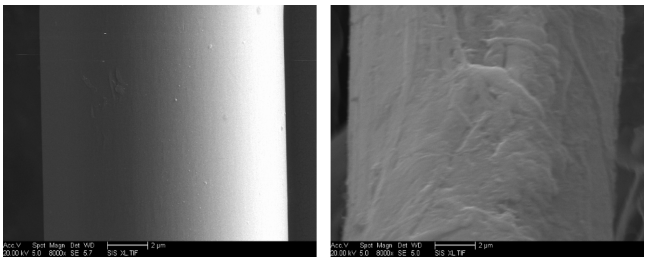

Figure 1. SEM images of the surface of an aramid fiber before (left) and after (right) being processed using dopamine.

(SEM) images of the surface of a poly(*p*-phenylene terephthalamide) (PPTA) fiber before and after being processed by dopamine. It is apparent that the polydopamine is well attached to the aramid fiber and that the polydopamine film layer roughs the surface of the smooth aramid fiber. The rough surface is conducive to the formation of a firm interface between the fiber and substrate and this, in turn, enhances the comprehensive performance of the composite. Surface processing of aramid fibers using dopamine also increases the variety of active functional groups on the chemically inert surface. Additionally, a polydopamine layer bearing eumelanin can absorb ultraviolet (UV) light and is thus conducive to improving the anti-UV aging performance of the aramid fiber. Although dopamine can effectively strengthen the surface performance of aramid fibers, the use of dopamine in the surface treatment of aramid fibers incurs a very high cost. To search for a dopamine substitute, it is necessary to explore the adhesion mechanism between dopamine and the surface of the aramid fiber.

It is generally thought that the unique adhesion ability of polydopamine is mainly sourced from its catechol groups[8] (or closely correlated *o*-quinoyl groups[12]). However, the definitive adhesion mechanism has not been made clear until now.[13] As polydopamine contains many active functional groups, the adhesion of polydopamine to other materials varies greatly and includes chemical connection and physical adhesion. The adhesion of polydopamine is closely correlated with the chemical structure or existing form of the substrate material. Different materials correspond to different adhesion mechanisms.[13] For materials containing amino or thiol groups on their surfaces, catechol groups develop aryl-alkylamine addition reactions based on Michael addition or Schiff base reaction.[8] The quinoyl groups in the polydopamine are prone to develop chemical reactions with nucleophiles (exemplified by the reaction between polydopamine and proteins[12]). Polydopamine can form covalent or noncovalent bonds with the material it adheres to due to the rich variety of functional groups possible. For example, there may be hydrogen bonding, π-stacking, and the complex mechanism of hydroquinone electron transfer.[13,14] The difficulty underlying the exploration of the adhesion mechanism in polydopamine lies in the complexity and diversity of the molecular structures of the polydopamine. Dopamine can be oxidized into a variety of monomer molecules in alkalescent aqueous solution. These include 5,6-dihydroxyindole (DHI) as a major component[15,16] and, to lesser extents, 5,6-indolequinone (IQ), leukodopaminechrome (LDPA),[17] and the different possible tautomers of DHI and LDPA.[17] These monomer molecules are polymerized into a variety of oligomer molecules by different linkage forms of bondings, which further gives rise to polydopamine with secondary structure as a result of noncovalent bonds.[18]

In the area of theoretical polymer physics, a molecular dynamics (MD) simulation method has proven to be an important tool to study the properties of polymers, because it provides a reliable approach to visualize polymers for detecting their specific functions and applications.[19−21] The MD simulation method is also qualified to investigate the density of polymers,[19,22−24] the polymer−polymer interfacial interactions,[25] the surface properties of polymers,[22,23,26,27] and the hydrogen-bonding interactions.[27,28] Using the MD simulation method, this study investigates the mechanism of adhesion between different structures including monomers, dimers, tetramers, and octamers on the surface of PPTA fiber. Using 21 typical polydopamine molecular structures, we analyze the density of the polydopamines with different molecular structures in the interface zone. We also find the work of adhesion between the two phases of the materials, etc. The results are used to explore the main molecular structures that play the major role in the polydopamine adhesion function. As the molecular structure of polydopamine is strongly influenced by the processing conditions, it may be supposed that optimum adhesion may be achieved by controlling these conditions. In addition, if polydopamine molecules with high adhesion ability can be synthesized on a large scale, then cheap surface-processing materials may possibly be forthcoming.

2. EXPERIMENTAL SECTION

2.1. Aramid Fiber Unit Cell Model. The surface of the aramid fiber considered here is composed of ideal Kevlar unit cells. Therefore, the initial, nonrelaxed Kevlar unit cell model used is the PPTA monoclinic crystal model proposed by Liu et al.[29] The parameters of the unit cell in this model are set as follows: a × b × c = 7.88 Å × 5.22 Å × 12.9 Å, and $\alpha = \beta = \gamma = 90°$. The full name of the structures space group is *P*1*a*1, which is simply recorded here as Pa. The point group is named as m, and the symmetry axis is b. The relative positions of the atoms in the repeating structural unit are expressed using the parameters given by the Northolt unit cell model.[30] Thus, the angles between the straight lines formed by the 1,4 carbon atoms of the phenylene groups in the terephthalic segment and the para-phenylenediamine segment with the *c*-axis are about 14 and 6°, respectively. The atoms of the amido group are coplanar. Moreover, the plane is parallel with the (100) plane and N−H···O hydrogen bonds (H-bonds) are generated. The angles between the amide plane and the terephthalic and *para*-phenylenediamine segments are −30 and 38°, respectively.

2.2. Polydopamine Molecules. Although the monomer molecules that compose the polydopamine are relatively few in number, the oligomers formed have many different molecular structures because the bonds formed between monomers vary considerably. Therefore, the polydopamine involved are, in fact, mixtures of many types of oligomers.[17,18,31] To analyze the role of the various molecular structures in the polydopamine in the adhesion process, 21 representative polydopamines varieties with independent molecular structures were taken into consideration. These are denoted using the form S*i* (*i* = 1, 2, ..., 21), and are shown in Figure 2.

In Figure 2, S4 is dopamine (DPA) and S1−S3 are its oxidized monomers DHI, IQ, and LDPA, respectively.[17] S5−S14 and S21 are the homopolymers of the monomer DHI through 2-, 4-, and 7-polymerization, respectively. S5−S10 are dimers, S11−S13 are tetramers, S14 is an octamer,[17,18] and S21 is an annular tetramer.[32] S15−S20 are copolymers generated by different monomers: S15 and

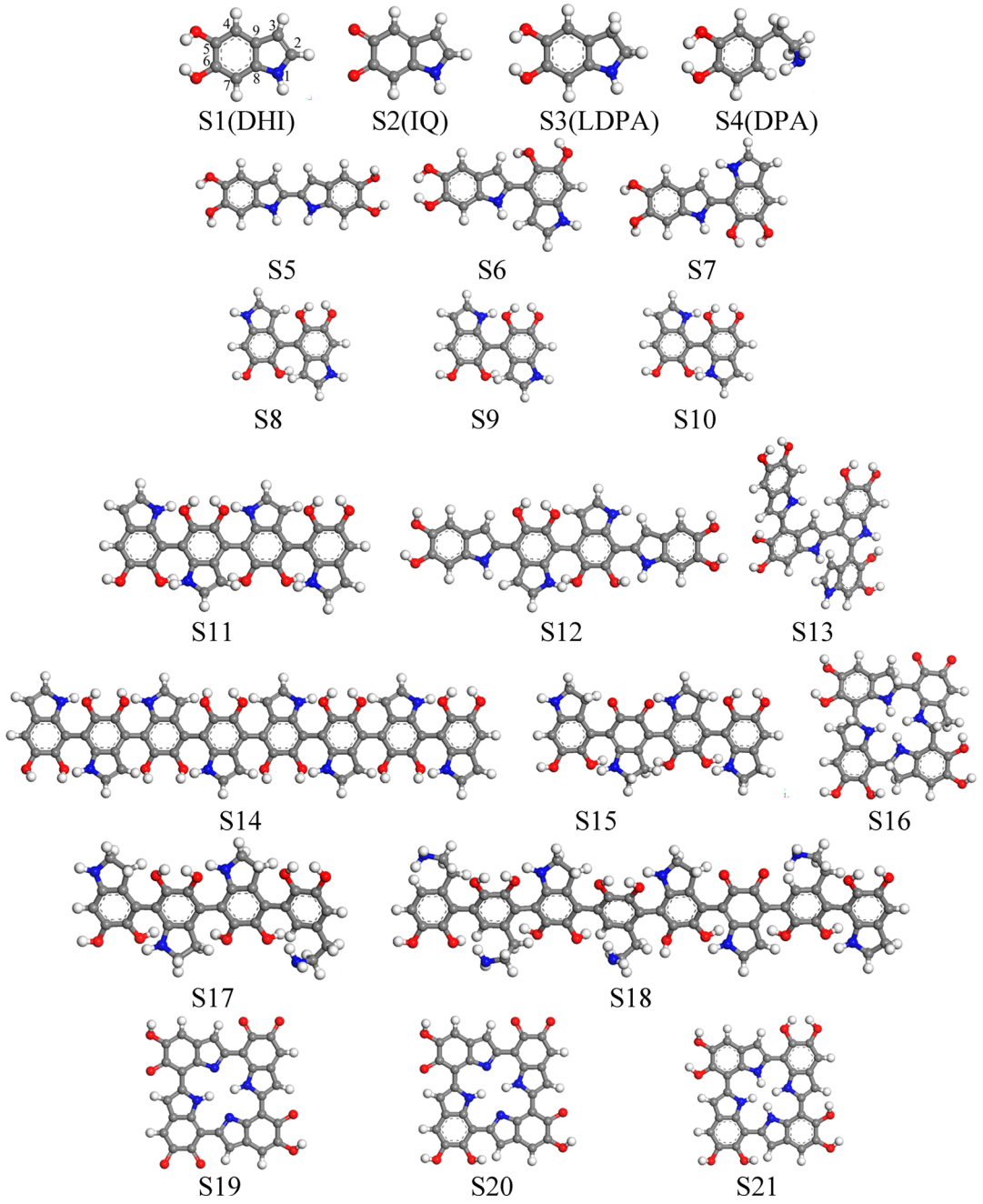

Figure 2. Representative molecular structures of the polydopamines[16−18,24,32] (dark gray balls correspond to C, white to H, blue to N, and red to O).

S16 are tetramers composed of one tautomer molecule of DHI and three LDPA molecules;[17] S17 is a tetramer synthesized by one DPA molecule and three LDPA molecules;[17] S18 is an octamer aggregated by one IQ molecule, three LDPA molecules, and four DPA molecules;[17] S19 is a tetramer synthesized by two IQ molecules and two quinone-methide (MQ) molecules;[16,24] and S20 is a tetramer polymerized from an IQ, a DHI molecule, and two MQ molecules.[16]

After the oxidized monomers of dopamine are polymerized into oligomers using covalent bonds, the oligomer molecules are aggregated into polydopamines using noncovalent bonds (van der Waals forces, H-bonds, and π-stacking).[17,33] The potential functions for the polydopamine molecules model were generated using a condensed-phase optimized molecular potentials for atomistic simulation studies (COMPASS) force field.[34,35] In the MD simulations, the initial density of the polydopamine was set to 1.079 g/cm^3 (which is smaller than the value 1.54 g/cm^3 calculated using Swift's theoretical model[36]). A smaller molecular density is selected because less molecular entanglement of the loose molecules helps the molecular system to achieve relaxation balance as quickly as possible.

2.3. MD Simulation of the Surface of the Aramid Fiber Modified by Polydopamines. Molecular simulation of the surface of the aramid fiber modified by polydopamines was conducted using the general COMPASS force field in Accelrys Materials Studio software. The process of simulating the molecular systems with 3080−3720 atoms proceeded as follows. First, a relaxed single unit cell of the aramid fiber was cleaved on the (100) plane to construct the unit-cell surface of an aramid fiber composed of seven layers of H-bonded sheets with 27.59 Å in height. The unit-cell surface was further extended to build the supercell surface. Here this plane was 25.81 Å long along the direction of the PPTA molecule chain, and 26.11 Å wide in the perpendicular direction. Second, a model of a unit cell of the polydopamine molecule was built. The size of the cross-section of the unit cell model of the polydopamine was exactly the same as the size of the surface of the aramid fiber. There were 80 monomers

constructed in a unit cell via the calculation of amorphous cell module to keep the size of cross section unchanged; and the height of the unit cell for all kinds of polydopamines was approximately 26.8 Å, which was determined by the initial density and the molecular structure. Finally, the two models obtained above were assembled into one unit cell and used as the initial model for the aramid fiber surface to be modified by polydopamines. The surface molecules of the aramid fiber in the unit cell were set as the first layer, while the polydopamine molecules above the aramid fiber were set as the second layer. One layer of vacuum with 600 Å in thickness was added above the second layer, but not between the first and second layers. The vacuum layer was large enough so that the Coulomb forces and the van der Waals forces between the periodic images on each side of vacuum had little effect on the results. After the vacuum layer was added, the molecules in the unit cell remained periodic in the tangential direction instead of the normal direction on the surface of the polydopamine. In the model built, the functions representing the H-bonds among the polydopamine molecules and the interface between the two phases of the materials were neglected. Finally, the Discover module was employed for the MD calculation. In the calculation, the charge effect of polydopamine molecules was taken into consideration. However, the overall charge on the molecules was zero. The integration time step was 1.0 fs and the cutoff distance for the noncovalent bond interactions was 15.5 Å.

To guarantee convergence of the calculation, a staged relaxation method was used. That is, stress relaxation in the asymmetric direction using an NVT ensemble was first achieved and then stress relaxation in the symmetrical direction using an NPT ensemble was realized. In addition, the "temperature-rising/annealing" calculation method was used to speed up exploration of the stable structures in the complex molecular model to reduce the calculation cost. The specific process used is as follows. First, smart minimization was used for static relaxation and 10 000 steps calculated to minimize the energy of the molecular structure. Then, keeping the temperature at 598 K using the NVT ensemble and controlling the temperature of the thermostat using Nose, relaxation was allowed for 0.03 ns. In turn, the system temperature was reduced to 298 K under the same conditions, and allowed to reach a relaxation balance using a further 0.03 ns of simulation. On this basis, H-bonds were added to perfect the molecular model and simulation conducted for 0.03 ns to achieve stress relaxation in the nonperiodic direction. Finally, under the NPT ensemble, the temperature was controlled at 298 K using the Andersen method and the pressure controlled using the Berendsen method. As there is a vacuum layer in the unit cell model, pressure could not be applied to the surface of the polydopamine. Therefore, 0.24 ns of simulation was carried out at zero pressure to achieve stress relaxation in each direction because the equilibrium was usually done within 30 ps in this stage, as indicated by the energy equilibrium of the S14−aramid system in Figure 3, for example. By making a statistical analysis of the total energy of the final relaxation model, the total energy of adhesion $E_{12,total}$ of the aramid fiber with the polydopamine can be obtained. S11−S21 can be smoothly simulated using the above simulation method. However, the method is not suitable for simulating S1−S10 as some of the molecules of S1−S10 may drift out of the unit cell at high temperatures. To avoid small molecules escaping at high temperatures, S5−S10 were simulated by employing a temperature of 498 K, whereas the temperature-rising and annealing method was not used for S1−S4.

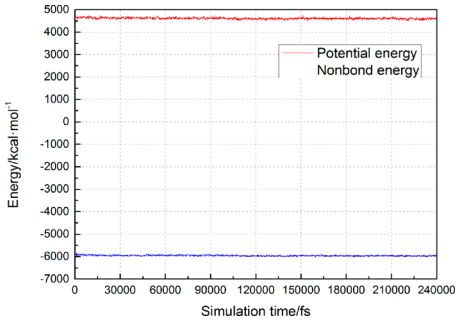

Figure 3. Potential energy and nonbond energy of S14−aramid system vs the simulation time.

Based on the above relaxation model, it is also possible to model a single polydopamine molecule by replacing the aramid fiber molecules with a vacuum layer. Using the same method, a molecular model of the aramid fiber can also be built. The molecular model of the aramid fiber or polydopamine was then placed under the NPT ensemble for 0.24 ns of relaxation at 298 K and 0 GPa. By making a statistical analysis of the total energy of the relaxed molecular model, the total energy of the aramid fiber $E_{1,total}$ and polydopamine $E_{2,total}$ could be obtained.

2.4. Calculation of the work of adhesion and surface energy. According to Young−Dupré equation,[37] the work of adhesion can be calculated using

$$W_{ad} = \alpha_1 + \alpha_2 - \alpha_{12} \quad (1)$$

where, α_1 and α_2 are the surface energies of the aramid fiber and polydopamine, respectively, and α_{12} is the interface energy. The energy of the aramid fiber and polydopamine, and the total energy of the whole bulk are defined using

$$\begin{aligned} E_{1,total} &= \alpha_1 A + E_{1,bulk} \\ E_{2,total} &= \alpha_2 A + E_{2,bulk} \\ E_{12,total} &= \alpha_{12} A + E_{1,bulk} + E_{2,bulk} \end{aligned} \quad (2)$$

Here, $E_{1,bulk}$ and $E_{2,bulk}$ are the energies of the adhesion systems of aramid fiber and polydopamine molecules in the MD model, respectively; A is the area of the interface. Using eq 2, eq 1 can be rewritten in the following form:

$$W_{ad} = \frac{1}{A}(E_{1,total} + E_{2,total} - E_{12,total}) \quad (3)$$

If a certain material was divided in two, then, on average, there would be $\alpha_{12} = 0$, $\alpha_1 = \alpha_2 = \alpha_0$, $E_{1,total} = E_{2,total} = E_{0,total}$, and $E_{12,total} = E_{00,total}$, and therefore,

$$W_{ad} = 2\alpha_0 = \frac{1}{A}(2E_{0,total} - E_{00,total}) \quad (4)$$

In this expression, α_0 is the surface energy, $E_{0,total}$ is the total energy of half of the molecular system after average division (including the surface free energy), and $E_{00,total}$ is the total energy of the material before the average division. The surface energy of the material can be calculated using the MD method by eq 4.

3. RESULTS AND DISCUSSION

3.1. Surface Energy of the Aramid Fiber. This study proposes using a favorable method of improving computational efficiency while maintaining computational accuracy. That is, we replace the aramid fiber surface with an appropriate number of layers of H-bonded sheets of PPTA. The number of layers required can be conveniently determined by calculating the surface energy of the H-bonded sheet system with different numbers of layers. On the basis of the relaxed Kevlar unit cell, the 2N layers of H-bonded sheets of PPTA are cleaved on the (100) plane to represent the Kevlar plane (N = 1, 3, 5, 7, 9, 20, and 50). Then, the unit cell of the aramid fiber surface is constructed by adding a vacuum layer above the aramid fiber model. The thicker the vacuum layer, the more accurate the representation of the surface separated by the aramid fiber being characterized. In this study, the thickness of the vacuum layer, H_{vac}, was set using the expression

$$H_{vac} = 100 + 10H_{solid} \quad (5)$$

Here, H_{solid} is the thickness of the nonvacuum part and equal to 7.88N (in Å). Thus, H_{vac} was 178.8 Å when N = 1.

Correspondingly, it was increased with increasing the layer number according to eq 5, so that the large thickness of the vacuum layer could ensure that the coulomb forces and the van der Waals forces between the periodic images on each side of vacuum had little effect on the results. The 2*N* layers of the H-bonded sheet of PPTA was divided into two shares, on average, with *N* layers in each share. Two new surfaces were thereby generated.

The aramid fiber surface before and after being divided (on average) were modeled using MD simulation. The atomic interactions and potential function in the aramid fiber unit cell were visualized using a COMPASS force field.[38] The total Hamiltonian of the unit cell at a temperature of 298 K and pressure of 0 GPa was calculated using the MD method. To realize complete relaxation of the molecular system as quickly as possible, NVT and NPT ensembles were employed for the calculation. During calculations using the NVT ensemble, the temperature was controlled using the Nose method. Moreover, the total simulation length was set to exceed 60 ps to eliminate the stress of the unit cell on the cleaved surface in the normal direction. For calculations using the NPT ensemble, the Andersen and Berendsen methods were used to control temperature and pressure, respectively. Again, the total simulation time was set to be longer than 60 ps. In this way, relaxation of the molecular system in all dimensions was finally realized. After obtaining the total energy of the molecular system, the surface energy of the aramid fiber was determined using eq 4.

Table 1 shows the relationship between the number of molecular layers and the surface energy of the PPTA aramid fiber. Clearly, as the number of layers increases, the surface energy tends to a fixed value, one which is actually close to the experimental value obtained by Hao et al.[39] By the seventh layer, the simulated surface energy of the aramid fiber has very nearly reached the convergent value. Therefore, the aramid fiber surface can be substituted by seven layers of H-bonded sheets.

Table 1. Relationship between the Number of Molecular Layers and the PPTA Surface Energy Simulated Using MD

	number of layers of aramid fiber molecules						
	1	3	5	7	9	20	50
surface energy (mJ/m^2)	22.9	25.6	27.2	30.6	30.1	30.1	29.7

3.2. Mechanism of Polydopamines Adhesion on the Surface of the Aramid Fiber. Because all the properties depend on the final structure of the molecular system, it is of great importance to ensure that the molecular structure has been properly relaxed. Moreover, the model size is one of the important parameters for the MD simulation. So, the simulations on four typical models with different sizes and times have been done to achieve the proper system size and simulation time. As can be seen in Table 2, there was little difference in work of adhesion between the present sizes and 3 times bigger sizes, as well as between the longer time than 0.24 ns and the 0.24 ns time. Therefore, all the discussions below are based on the equilibrium results of the present molecular system with relaxation simulation for 0.24 ns.

Assuming that there are no chemical reactions between the polydopamines and aramid fiber, the polydopamine molecules with shorter chains can adhere to the surface of the aramid fibers through intermolecular interactions (e.g., van der Waals forces). To the authors' knowledge, there was little information available in literature about the covalent bonding between the dopamine and the surface of aramid fiber. The future work will demonstrate the types of bonding between these two systems. The MD simulation results show that, in addition to van der Waals forces, there are rich H-bonds and π-stacking between the polydopamines and the surface of the aramid fiber. These are very conducive to polydopamine molecules approaching the surface of the aramid fibers.

Table 2. Work of Adhesion of the Polydopamines on the Surface of Aramid Fiber with Different Sizes and Times in MD Simulations

periodic molecular system	size of the interface, $Y \times Z$ ($Å^2$)	relaxation time in the last stage (ns)	work of adhesion (mJ/m^2)
S10−aramid	26.11 × 25.81 (present)	0.24 (present)	40.67
S10−aramid	26.11 × 25.81	0.74	40.12
S10−aramid	52.22 × 51.62	0.74	39.30
S11−aramid	26.11 × 25.81 (present)	0.24 (present)	39.43
S11−aramid	26.11 × 25.81	0.74	39.24
S11−aramid	52.22 × 51.62	0.74	38.22
S14−aramid	26.11 × 25.81 (present)	0.24 (present)	28.29
S14-aramid	26.11 × 25.81	0.74	27.95
S14−aramid	52.22 × 51.62	0.74	29.65
S19−aramid	26.11 × 25.81 (present)	0.24 (present)	49.78
S19−aramid	26.11 × 25.81	0.74	50.07
S19−aramid	52.22 × 51.62	0.74	50.33

H-bonds are readily formed around the N and O atoms[27,28] in the interface between the aramid fiber surface and polydopamines, mainly in these forms: O−H···O, O−H···N, N−H···O, and N−H···N (Figure 4). The O−H groups involved are mainly present in S1, S3, S4, MQ, and the

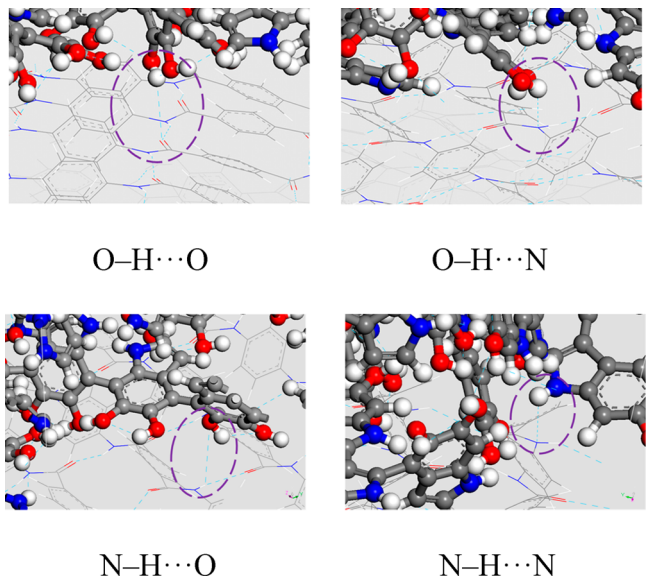

Figure 4. H-bonds between PDA and aramid fibers. (The ball-and-stick model in the upper part represents the polydopamines, whereas the linear model in the lower part represents the surface of the PPTA fiber.)

hydroxyl groups in the polymers of MQ. N−H are mainly found as donors including the indolyl groups in S1 and S2 and the amino groups in S4. H-bonds are mainly received by the O and N atoms in the aramid fibers. In addition, H-bonds can also be formed by the N−H groups in the aramid fibers and the O atoms in polydopamine molecules. As hydroxyl-rich DHI is the main component in the polydopamines, the first two forms of the four forms of H-bonds are more prevalent than the latter two.

As there are a lot of annular benzene rings present, π-stacking can be readily formed between aramid fibers and polydopamines. Depending on the polymerization in the molecular chains of the polydopamines, the molecular chains of low-molecular weight polydopamines are completely or partly distributed on the surface of the rigid aramid fiber molecules. Simulations using DHI molecules with different polymerization degrees reveal that as the polymerization degree of the DHI increases, the number of chain segments of the polydopamines gradually decreases in the spatial range with a thickness of 8.5 Å (including the surface atoms that compose the first sheet of the aramid fiber). Some complete chains of the dimer and tetramer are tiled on the surface of the aramid fiber. Most chain segments of the octamer were restricted by other molecules, so only part of the chain segments were tiled on the surface of the aramid fiber, as shown in Figure 5. Obviously, the lower the

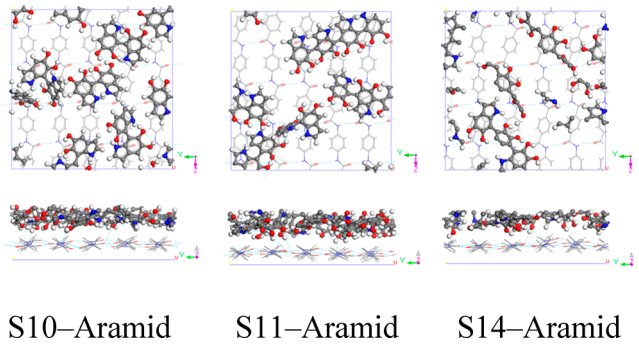

Figure 5. Cross-sectional view of the π-stacking between the aramid fiber surface and different polydopamine molecules.

polymerization degree, the shorter the molecular chains, and thus the molecular chains can more easily approach the aramid fiber molecules and successfully generate π-stacking.

Some annular molecules with a polymerization degree of 4 are distributed on the surface of the aramid fiber surface and develop into π-stacking. S21 (annular molecules composed of 4 DHIs) has an annular structure with a curved surface. As each such structure increases the strain among molecules, the aggregation form becomes a mess. The annular molecule S19 and the annular eumelanin molecule S20 have planar annular structures and can stack neatly on the surface of the aramid fiber (Figure 6). The reason for this lies in the fact that the two adjacent indole molecules are restricted in the same plane by the N=C bonds in the two molecular structures. Compared with polydopamine molecules with curved annular surfaces, planar annular eumelanin molecules are more prone to π-stacking. The stacking forms of S19 and S20 on the surface of the aramid fiber are consistent with the eumelanin distribution law simulated by Buehler et al.[24]

The simulations above merely relate to one key link in the dopamine polymerization process. Further oxidation and cross-linking of the small polydopamine molecules adhering to the

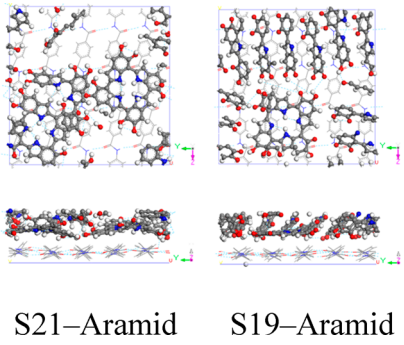

Figure 6. Cross-sectional view of the π-stacking between the aramid fiber surface and annular polydopamine molecules.

surface of the aramid fiber causes a nanometer-thick cross-linked layer to form. This layer strengthens the integrity of the adhesion effect of the polydopamine film layer. Meanwhile, a melanin shell of nanometer thickness is formed on the whole surface of the aramid fiber. The organic shell provides a certain rigidity and can thus restrict and protect the aramid fiber.

3.3. Morphology and Density Distribution of the Polydopamines in the Interface Region. The simulation results show that the molecular chains in the aramid fiber unit cell are very rigid. The H-bonded sheet basically keeps a constant shape from beginning to end and this provides a smooth and stable surface for the adhesion of polydopamines. The unrestricted parts of the small polydopamine molecules (independent small molecules or dangling molecular chains) display greater motional flexibility and ability to deform. After relaxation, the initially loose polydopamine molecules adhere compactly to the surface of the aramid fiber. That is to say, the polydopamines composed of oligomers proactively adhere to the surface of the aramid fiber. After relaxation, a relatively smooth surface is formed between the polydopamine nanofilm layer and aramid fiber surface, as shown in Figure 7.

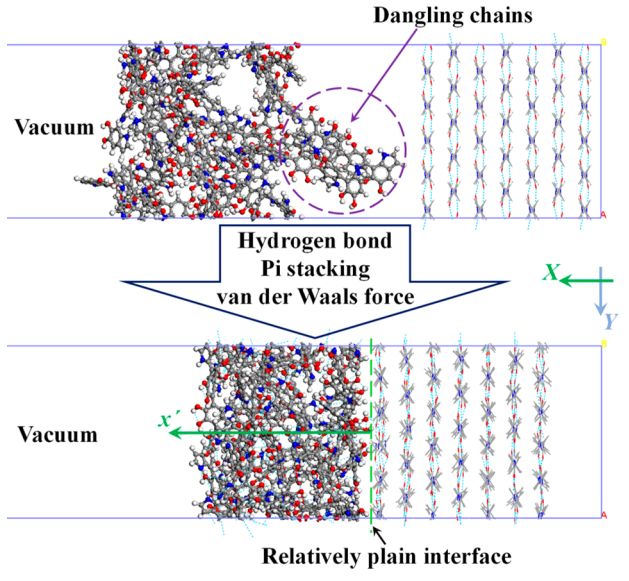

Figure 7. Lateral view of a polydopamine composed of the octamer of DHI adhering to an aramid fiber surface. (The ball-and-stick model on the left represent polydopamine nanofilm layer, whereasthe linear models on the right refer to the surface of the PPTA fiber.)

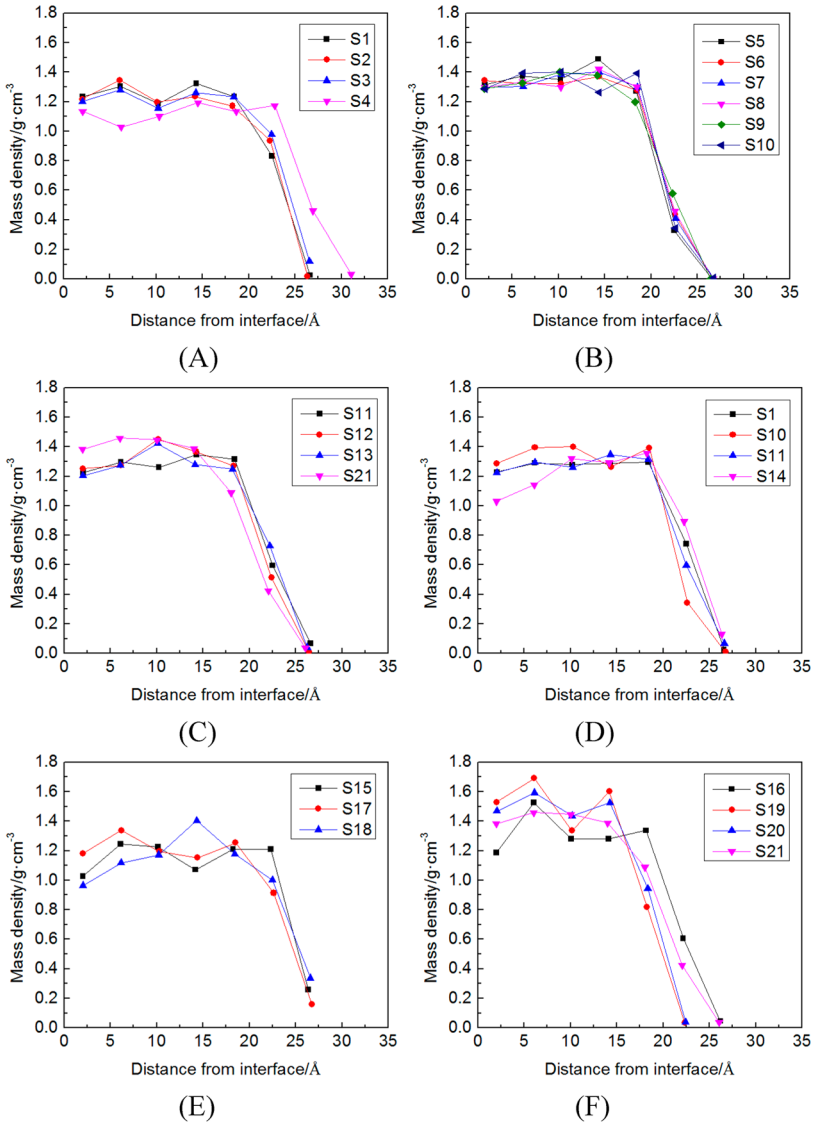

Figure 8. Atomic density distributions of the polydopamines in the interfacial region.

As the molecular chains of the polydopamine adhering to the aramid fiber surface have different structures, the structures of the interfacial layers are different. The density distribution of the aramid fiber and polydopamine on the two sides of the interface effectively reflect the degree of contact between the two phases of the material in the interface zone. In agreement with the relationship between the position of the polydopamine and aramid fiber in Figure 7, a regional atomic mass density of the aramid fiber modified by polydopamine can be defined. Using a new coordinate axis, x', whose origin is a point in the interface and whose positive direction is identical to the that of the X-axis, the regional atomic mass density ρ_i is defined as

$$\rho_i = \frac{m_{r_{i-1},r_i}}{V_{r_{i-1},r_i}}, \quad r_i = iR \ (i = -6, -5, ..., 6, 7) \tag{6}$$

where m_{r_{i-1},r_i} and V_{r_{i-1},r_i} are the density and total atomic mass in the volume of space in the interval (r_{i-1},r_i), respectively. Also, R is the distance between two adjacent layers of H-bonded sheets of the aramid fiber and r_i refers to the offset along the normal direction of the interface with the interface position as the starting point. The variable i, when positive, represents the PDA region and the aramid fiber region, when nonpositive.

The calculation results show that the atomic density distribution essentially stays at 1.42 ± 0.02 g/cm^3 in the aramid fiber region. In the polydopamine distribution region, the density distribution is nonuniform. As shown in Figure 8, the density distribution of the polydopamines can be divided into three main parts: V_{r_0,r_2} near the interface, V_{r_2,r_5} in the middle region, and V_{r_5,r_7} in the surface region.

The first point (from left to right) of each curve in this region corresponds to ρ_1, the second point to ρ_2, etc. The region near the interface and middle region, namely V_{r_0,r_5}, are both considered to be the main polydopamine film region. Figure 8A shows the density distribution of the structural composition of four monomers, DHI, IQ, LDP, and DPA. In the interface region of the polydopamine film layer, the densities of S1−S3 exceed that of S4. When i = 2, the simulated density of the four monomers are clearly different. S2 presents the highest density (1.34 g/cm^3), followed by S1 (1.30 g/cm^3). The density of S3 is next (1.27 g/cm^3) followed by S4 with the lowest density (1.02 g/cm^3). The reason why the densities of

Table 3. Work of Adhesion of the Polydopamines with Different Molecular Structures on the Surface of Aramid Fiber

polydopamine	work of adhesion (mJ/m^2)	polydopamine	work of adhesion (mJ/m^2)	polydopamine	work of adhesion (mJ/m^2)
S1 (DHI)	49.01	S8	39.63	S15	22.06
S2 (IQ)	53.35	S9	40.81	S16	31.24
S3 (LDPA)	44.98	S10	40.67	S17	23.91
S4 (DPA)	29.54	S11	39.43	S18	26.70
S5	49.17	S12	45.82	S19	49.78
S6	46.90	S13	36.02	S20	45.49
S7	39.58	S14	28.29	S21	37.36

S1−S3 are higher than that of S4 lies in the cyclic structure formed by the branched chains of the initial ethylamine, which reduces the space occupied by molecules. In contrast, for S4 (i.e., DPA), the branched chains of the ethylamine expand the space occupied by molecules.

Figure 8B shows the density distribution in the polydopamines aggregated by the dimers of DHI. When i = 1, the maximum density of 1.34 g/cm^3 and minimum of 1.29 g/cm^3 are found in S6 and S9, respectively, a difference of 0.05 g/cm^3. It can be seen that the densities of S5−S10 are very close. In addition, the density of dimers in region V_{r_0,r_1} is slightly affected by the linkage forms of bondings. This is attributed to the fact that the molecules in the various structures can distribute themselves uniformly on the surface of the aramid fiber due to weak entanglement and binding effects among the dimer molecules. When i = 4, the polydopamines aggregated by the different molecules show the maximum density difference of 0.23 g/cm^3. S5 and S10 display the maximum (1.49 g/cm^3) and minimum densities (1.26 g/cm^3), respectively. The reason lies for this is that the (2,2′) bond of S5 has no free rotation and the C atoms in the whole molecule are coplanar. This structure is conducive to molecular stacking. In contrast, the planes of the two structural units of S6−S10 present certain angles. Such structures increase the spatial volume and reduce the density of the molecules.

Figure 8C illustrates the aggregated atomic density distribution of the tetramers of DHI on the surface of the aramid fiber. When i = 1 and 2, the density of S21 surpasses those of S11−S13. This is because the annular molecules of tetramer S21 form a curved surface structure that can stack together, while the crisscrossed, chain-like S11−S13 molecules fail to achieve a high spatial utilization rate. The simulation results suggest that the whole of the molecular structure of the chain-like tetramer is distributed on the surface of the aramid fiber (Figure 5). This result suggests that the molecular aggregation of the tetramer is less restricted by other molecules and it can thus distribute itself relatively uniformly on the surface of the aramid fiber. As a result, S11−S13 show closely related densities in the interface region. When i = 3, the densities of S12 and S13 are higher than that of S11. At this point, the straight-chain-like S12 molecules combine favorably spatially, while S13 molecules with a curved structure stack together in pairs. Such stacking increases the density in this region.

Figure 8D illustrates the density distribution of chain-like polydopamines generated by DHI with different degrees of polymerization on the surface of the aramid fiber. When i = 1, the atomic densities of S10, S11, and S14 are 1.37, 1.22, and 1.03 g/cm^3, respectively. That is to say, the atomic density of the chain-like polydopamines on the surface of the aramid fiber decreases with an increase in the degree of polymerization. This is because if the degree of polymerization is high, the molecular chains of the polydopamine molecules are entangled and their interactions restricted so that the molecules cannot make close contact with the surface of the aramid fiber. The free space in the interface is thereby expanded. When i = 1, it is not that strange that the density of S10 (1.37 g/cm^3) exceeds the density of S1 (1.23 g/cm^3). First, as S10 is a polymerized form of S1, and is free of entanglement and restriction, it can distribute itself densely on the surface of the aramid fiber. Second, under the premise there is the same amount of structural units, the repulsive force among the single molecules of S1 is greater than that between S10 dimers. As a result, the spatial volume of S1 is larger than that occupied by S10.

Figure 8E shows the atomic density distribution of chain-like copolymers S15, S17, and S18 on the interface of aramid fibers. It can be seen that the atomic densities of S15, S17, and S18 differ greatly. When i = 1 and 2, tetramers S15 and S17 present a density that is greater than that of octamer S18. Therefore, like the distribution law for the chain-like homopolymers, the distribution density of the chain-like copolymers decreases with the degree of polymerization.

Figure 8F shows the atomic density distribution of annular copolymers S16, S19, S20, and S21 on the interface of the aramid fiber. When i = 1, the densities of S19 and S20 are 1.53 and 1.47 g/cm^3, respectively. Both of these are larger than those of S16 (1.18 g/cm^3) and S21 (1.38 g/cm^3). The reason for this lies in the fact that the molecular structures of S19 and S20 are approximately rigid planes on the whole. Such a structure facilitates neat and dense stacking of molecules on the surface. In contrast, the relative rotation between the polymerization units of S16 and S21 makes them prone to form twisted curved surfaces, which goes against the effective utilization of space.

To sum up, the polydopamine density approximately lies in a range of 1.03−1.69 g/cm^3 in the interfacial region. The neater the structure and the lower the degree of polymerization, the more concentrated the molecules on the interface (e.g., S2, S5, and S19). In addition, regardless of whether they are long, flexible molecular chains or short, rigid molecular chains, the dopamine oligomers can form a dense interface with the aramid fiber surface. This helps the formation of noncovalent bonds between the two phases of material.

3.4. Work of Adhesion of Polydopamines. The work of adhesion is an important parameter for characterizing the adhesion strength between two phases of material. Due to the complex structures of the polydopamines, different molecular structures correspond to disparate interfacial structures and, therefore, works of adhesion. In this study, the MD method is employed to calculate the work of adhesion for the 21 typical kinds of polydopamines on the surface of an aramid fiber. Table 3 lists the results. The work of adhesion of the four monomers S1−S4 decrease in the sequence S2 > S1 > S3 > S4. The high adhesive strength of the alkalescent solution of polydopamine in the initial stage is closely correlated with the oxidized

structure of the dopamine. The work of adhesion of IQ, DH, and LDPA are 81%, 66%, and 52% larger than that of DPA. The reason for this lies in the closed-ring structure formed by the initial branched chains of ethyl ammonia after DPA oxidization reduces the space occupied by molecules. Therefore, molecules can more readily draw closer to the surface of the aramid fiber and thereby engage in H-bond and π-stacking, finally resulting in a large work of adhesion. Due to its two =O bonds, IQ shows a flatter molecular structure than DHI and thus attains a higher work of adhesion. As there are annular indole structures in the molecules of IQ and DHI, the molecules are very flat and compact, and the densely distributed molecules occupy a small amount of space. Moreover, the H-bonds in the annular lateral groups belonging to LDPA destroy the flatness of the molecular structure. As DPA does not generate indole groups, its molecules occupy a large amount of space and this hinders the approach of molecular chains to the aramid fiber's surface.

Due to the different ways to link it, DHI dimers can produce different molecular structures, resulting in different works of adhesion. Comparison of the calculation results for S5−S10 reveals that S5 presents the largest work of adhesion. This is because the coplanar structure of the two DHI units in S5 molecular increase the contact area between S5 and the aramid fiber surface. In contrast, all the other dimers have spatial structures with two DHI units rotated to a certain degree around the covalent bond that links the two DHI units, and thus present a smaller area of projection on the surface of the aramid fiber.

Comparison of the work of adhesion of the tetramers of DHI (S11, S12, and S13) discloses that S12 displays the largest work of adhesion. This is because the interaction area is increased, as S12 can stretch on the surface of the aramid fiber due to its long molecular chain and overall high flexibility. The molecular structure of S13 is twisted into a spiral, curved surface structure. Molecules of S13 therefore occupy a larger space and this hinders contact with the aramid fiber surface. Compared to the chain-like molecules, the annular S21 molecule does not contain two free ends and shows an annular structure with a curved surface. Such a structure increases the mismatch between the molecules and thus restricts the aggregation of them. The disordered distribution of S21 molecules reduces the effective area of projection on the aramid fiber surface (Figure 6). Therefore, S21 and S13 have relatively low works of adhesion.

Comparison of the work of adhesion of DHI with those of dimers S5−S10, tetramers S11−S13 and S21, and octamer S14 reveals that the straight-chain-like dimer S5 has the largest work of adhesion. Octamers present the smallest work of adhesion and those of the tetramers are slightly less than those of the initial dimers. Obviously, when the polymerization degree is more than 2, an increase in degree of polymerization may weaken the work of adhesion. The reason is that long molecular chains hinder the formation of a smooth and neat surface as they roughen the surface contact and interfere with each other. The more prolonged the oxidation of dopamine in air, the greater the polymerization degree and the more complex the aggregation structure of the molecules. As a result, the dopamine finds it harder to adhere strongly to the fiber's surface.

Among the oligomers (from S10 to S21), S19 and S20 show prominent work of adhesion values, 49.78 and 45.49 mJ/m^2, respectively. These high values are closely correlated with the planar annular structure of S19 and S20. In contrast to the curved annular surface structures in S21 and S16, the two quinone-methide structures in the molecules of S19 and S20 define the molecular configuration as planar. The planar structure effectively avoids intermolecular entanglement. Therefore, S19 and S20 can stack more neatly and orderly on the surface of the aramid fiber throughout the entire polydopamine layer compared to the other oligomer molecules. In turn, the noncovalent bonds between the two phases of material can connect with each other more readily. As a result, the work of adhesion of S19 and S20 are relatively high. Compared to S19, the two extra H atoms in the molecular configuration S20 make it less likely to form a planar annular structure. Therefore, the work of adhesion of S20 is less than that of S19. In addition, S16 molecules are also annular tetramers. However, the simulation results reveal that the molecular structure of S16 transforms into spatial structures with "N' or 'S" shapes. Such structures restrict the effective contact between the S16 molecules and aramid fiber surface. Therefore, the work of adhesion of S16 is reduced.

To sum up, IQ has the highest work of adhesion, followed by the annular eumelanin molecule S19 with annular plane structure. Among the DHI oligomers, dimer S5 proved to be the molecule with the best adhesion ability. Therefore, there is reason to suppose that the three above types of molecular structure can be used to process the surface of aramid fiber using dopamine and by controlling the processing conditions. Increasing the quantity of these three types of molecular structure is helpful in improving the ability of the dopamine to adhere to the surface of the aramid fiber.

4. CONCLUSIONS

This study first constructs an all-atomic model of an aramid fiber surface modified by dopamine using Accelrys Material Studio software and a COMPASS force field. It is used to analyze the mechanism of adhesion of the polydopamines aggregated by 21 typical kinds of molecular structure on the surface of the aramid fiber. The MD simulation results show that a clear and smooth interface is formed between the polydopamine nanofilms and the aramid fiber surface. In the small interfacial region, the polydopamines have a high atomic density, which is conducive to noncovalent bond between the polydopamine and aramid surface (van der Waals forces, H-bonds, and π-stacking). Then we investigated the work of adhesion of the 21 structures on the surface of the aramid fiber. The results prove that IQ shows the largest work of adhesion, followed by eumelanin molecules (S19) with a planar annular structure. The dimer S5 proved to be the molecule with the best adhesion ability among the DHI oligomers. The degree of polymerization strongly affects the work of adhesion. As the polymerization degree increases to 8, the work of adhesion suddenly drops. Therefore, the longer the dopamine is oxidized in air, the greater the degree of polymerization, and the harder it is for the dopamine to adhere to the fiber surface.

AUTHOR INFORMATION

Corresponding Authors

*Z. Xie. E-mail: xiezhm@hit.edu.cn.
*Y. Wang. E-mail: wangys@hit.edu.cn.

Author Contributions

The paper was written through contributions of all authors. All authors have given approval to the final version of the paper.

Notes

The authors declare no competing financial interest.

■ ACKNOWLEDGMENTS

The authors gratefully acknowledge financial support by the National Science Foundation of P. R. China under Projects No. 10972068 and No. 51173032. The authors also thank Mr. Qingliang Dong for his help in the experiment on the aramid fiber surface modified by DPA.

■ ABBREVIATIONS

COMPASS , condensed-phase optimized molecular potentials for atomistic simulation studies
DHI , 5,6-dihydroxyindole
DPA , dopamine
IQ , 5,6-indolequinone
LDPA , leukodopaminechrome
MD , molecular dynamics
MQ , quinone-methide
PDA , polydopamine
PPTA , poly(*p*-phenylene terephthalamide)

■ REFERENCES

(1) Lin, J. S. Effect of Surface Modification by Bromination and Metalation on Kevlar Fibre-Epoxy Adhesion. *Eur. Polym. J.* **2002**, *38*, 79−86.
(2) Mori, M.; Uyama, Y.; Ikada, Y. Surface Modification of Aramid Fiber by Graft Polymerization. *Polymer* **1994**, *35*, 5336−5341.
(3) Sun, D. M.; Chen, X. G. Plasma Modification of Kevlar Fabrics for Ballistic Applications. *Text. Res. J.* **2012**, *82*, 1928−1934.
(4) Zhang, Y.; Jiang, Z.; Huang, Y.; Li, Q. The Modification of Kevlar Fibers in Coupling Agents by γ-ray Co-irradiation. *Fibers Polym.* **2011**, *12*, 1014−1020.
(5) Liu, L.; Huang, Y. D.; Zhang, Z. Q.; Jiang, Z. X.; Wu, L. N. Ultrasonic Treatment of Aramid Fiber Surface and Its Effect on the Interface of Aramid/Epoxy Composites. *Appl. Surf. Sci.* **2008**, *254*, 2594−2599.
(6) Xi, M.; Li, Y. L.; Shang, S. y.; Li, D. H.; Yin, Y. X.; Dai, X. Y. Surface Modification of Aramid Fiber by Air DBD Plasma at Atmospheric Pressure with Continuous On-Line Processing. *Surf. Coat. Technol.* **2008**, *202*, 6029−6033.
(7) Biswas, M. A. K.; Shayed, M. A.; Hund, R. D.; Cherif, C. H. Surface Modification of Twaron Aramid Fiber by the Atmospheric Air Plasma Technique. *Text. Res. J.* **2013**, *83*, 406−417.
(8) Lee, H.; Dellatore, S. M.; Miller, W. M.; Messersmith, P. B. Mussel-Inspired Surface Chemistry for Multifunctional Coatings. *Science* **2007**, *318*, 426−430.
(9) Wang, W.; Li, R.; Tian, M.; Liu, L.; Zou, H.; Zhao, X.; Zhang, L. Surface Silverized meta-Aramid Fibers Prepared by Bio-inspired Poly(dopamine) Functionalization. *ACS Appl. Mater. Interfaces* **2013**, *5*, 2062−2069.
(10) Hu, H.; Yu, B.; Ye, Q.; Gu, Y.; Zhou, F. Modification of Carbon Nanotubes with a Nanothin Polydopamine Layer and Polydimethylamino-ethyl Methacrylate Brushes. *Carbon* **2010**, *48*, 2347−2353.
(11) Chen, S.; Cao, Y.; Feng, J. Polydopamine as an Efficient and Robust Platform to Functionalize Carbon Fiber for High-Performance Polymer Composites. *ACS Appl. Mater. Interfaces* **2013**, *6*, 349−356.
(12) Lee, H.; Rho, J.; Messersmith, P. B. Facile Conjugation of Biomolecules onto Surfaces via Mussel Adhesive Protein Inspired Coatings. *Adv. Mater.* **2009**, *21*, 431−434.
(13) Liu, Y.; Ai, K.; Lu, L. Polydopamine and Its Derivative Materials: Synthesis and Promising Applications in Energy, Environmental, and Biomedical Fields. *Chem. Rev.* **2014**, *114*, 5057−5115.
(14) Dreyer, D. R.; Miller, D. J.; Freeman, B. D.; Paul, D. R.; Bielawski, C. W. Elucidating the Structure of Poly(dopamine). *Langmuir* **2012**, *28*, 6428−6435.
(15) Panzella, L.; Gentile, G.; D'Errico, G.; Della Vecchia, N. F.; Errico, M. E.; Napolitano, A.; Carfagna, C.; d'Ischia, M. Atypical Structural and π-Electron Features of a Melanin Polymer That Lead to Superior Free-Radical-Scavenging Properties. *Angew. Chem., Int. Ed.* **2013**, *52*, 12684−12687.
(16) Meng, S.; Kaxiras, E. Theoretical Models of Eumelanin Protomolecules and Their Optical Properties. *Biophys. J.* **2008**, *94*, 2095−2105.
(17) Liebscher, J.; Mrowczynski, R.; Scheidt, H. A.; Filip, C.; Hadade, N. D.; Turcu, R.; Bende, A.; Beck, S. Structure of Polydopamine: A Never-Ending Story? *Langmuir* **2013**, *29*, 10539−10548.
(18) d'Ischia, M.; Napolitano, A.; Pezzella, A.; Meredith, P.; Sarna, T. Chemical and Structural Diversity in Eumelanins: Unexplored Bio-optoelectronic Materials. *Angew. Chem., Int. Ed.* **2009**, *48*, 3914−3921.
(19) Jawalkar, S. S.; Adoor, S. G.; Sairam, M.; Nadagouda, M. N.; Aminabhavi, T. M. Molecular Modeling on the Binary Blend Compatibility of Poly(vinyl alcohol) and Poly(methyl methacrylate): An Atomistic Simulation and Thermodynamic Approach. *J. Phys. Chem. B* **2005**, *109*, 15611−15620.
(20) Jawalkar, S. S.; Aminabhavi, T. M. Molecular Modeling Simulations and Thermodynamic Approaches to Investigate Compatibility/Incompatibility of Poly(L-lactide) and Poly(vinyl alcohol) Blends. *Polymer* **2006**, *47*, 8061−8071.
(21) Jena, K. K.; Raju, K. V. S. N.; Prathab, B.; Aminabhavi, T. M. Hyperbranched Polyesters: Synthesis, Characterization, and Molecular Simulations. *J. Phys. Chem. B* **2007**, *111*, 8801−8811.
(22) Prathab, B.; Aminabhavi, T. M.; Parthasarathi, R.; Manikandan, P.; Subramanian, V. Molecular Modeling and Atomistic Simulation Strategies to Determine Surface Properties of Perfluorinated Homopolymers and Their Random Copolymers. *Polymer* **2006**, *47*, 6914−6924.
(23) Prathab, B.; Aminabhavi, T. M. Atomistic Simulations to Compute Surface Properties of Poly(N-vinyl-2-pyrrolidone) (PVP) and Blends of PVP/Chitosan. *Langmuir* **2007**, *23*, 5439−5444.
(24) Chen, C. T.; Ball, V.; de Almeida Gracio, J. J.; Singh, M. K.; Toniazzo, V.; Ruch, D.; Buehler, M. J. Self-Assembly of Tetramers of 5,6-Dihydroxyindole Explains the Primary Physical Properties of Eumelanin: Experiment, Simulation, and Design. *ACS Nano* **2013**, *7*, 1524−1532.
(25) Prathab, B.; Subramanian, V.; Aminabhavi, T. M. Molecular Dynamics Simulations to Investigate Polymer−Polymer and Polymer−Metal Oxide Interactions. *Polymer* **2007**, *48*, 409−416.
(26) Prathab, B.; Subramanian, V.; Aminabhavi, T. M. Computation of Surface Energy and Surface Segregation Phenomena of Perfluorinated Copolymers and Blends − A Molecular Modeling Approach. *Polymer* **2007**, *48*, 417−424.
(27) Prathab, B.; Aminabhavi, T. M. Molecular Modeling Study on Surface, Thermal, Mechanical and Gas Diffusion Properties of Chitosan. *J. Polym. Sci., Part B: Polym. Phys.* **2007**, *45*, 1260−1270.
(28) Jawalkar, S. S.; Raju; Halligudi, S. B.; Sairam, M.; Aminabhavi, T. M. Molecular Modeling Simulations to Predict Compatibility of Poly(vinyl alcohol) and Chitosan Blends: A Comparison with Experiments. *J. Phys. Chem. B* **2007**, *111*, 2431−2439.
(29) Liu, J.; Cheng, S. Z. D.; Geil, P. H. Morphology and Crystal Structure in Single Crystals of Poly(*p*-phenylene terephthalamide) Prepared by Melt Polymerization. *Polymer* **1996**, *37*, 1413−1430.
(30) Northolt, M. G.; van Aartsen, J. J. On the Crystal and Molecular Structure of Poly-(*p*-phenylene terephthalamide). *J. Polym. Sci., Polym. Lett. Ed.* **1973**, *11*, 333−337.
(31) Della Vecchia, N. F.; Avolio, R.; Alfe, M.; Errico, M. E.; Napolitano, A.; d'Ischia, M. Building-Block Diversity in Polydopamine underpins a Multifunctional Eumelanin-Type Platform Tunable through a Quinone Control Point. *Adv. Funct. Mater.* **2013**, *23*, 1331−1340.
(32) Kaxiras, E.; Tsolakidis, A.; Zonios, G.; Meng, S. Structural Model of Eumelanin. *Phys. Rev. Lett.* **2006**, *97*, 218102.
(33) Lin, S.; Chen, C. T.; Bdikin, I.; Ball, V.; Gracio, J.; Buehler, M. J. Tuning Heterogeneous Poly(dopamine) Structures and Mechanics: In

Silico Covalent Cross-Linking and Thin Film Nanoindentation. *Soft Matter* **2014**, *10*, 457−464.
(34) Sun, H.; Ren, P.; Fried, J. R. The COMPASS Force Field: Parameterization and Validation for Phosphazenes. *Comput. Theor. Polym. Sci.* **1998**, *8*, 229−246.
(35) Raghu, A. V.; Gadaginamath, G. S.; Jawalkar, S. S.; Halligudi, S. B.; Aminabhavi, T. M. Synthesis, Characterization, and Molecular Modeling Studies of Novel Polyurethanes Based on 2,2′-[Ethane-1,2-diylbis(nitrilomethylylidene)]diphenol and 2,2′-[Hexane-1,6-diylbis-(nitrilomethylylidene)] Diphenol Hard Segments. *J. Polym. Sci., Part A: Polym. Chem.* **2006**, *44*, 6032−6046.
(36) Swift, J. A. Speculations on the Molecular Structure of Eumelanin. *Int. J. Cosmet. Sci.* **2009**, *31*, 143−150.
(37) Finnis, M. W. The Theory of Metal-Ceramic Interfaces. *J. Phys.: Condens. Matter* **1996**, *8*, 5811−5836.
(38) Grujicic, M.; Glomski, P. S.; Pandurangan, B.; Bell, W. C.; Yen, C. F.; Cheeseman, B. A. Multi-Length Scale Computational Derivation of Kevlar® Yarn-Level Material Model. *J. Mater. Sci.* **2011**, *46*, 4787−4802.
(39) Hao, W. F.; Yao, X. F.; Ke, Y. C.; Ma, Y. J.; Li, F. X. Experimental Characterization of Contact Angle and Surface Energy on Aramid Fibers. *J. Adhes. Sci. Technol.* **2013**, *27*, 1012−1022.